

## Morphological, Structural and Optical Properties of Er<sup>3+</sup>-Doped SiO<sub>2</sub>-TiO<sub>2</sub> Nanofiber

Nurul Syaheera Razali 1<sup>a</sup>, Siti Nurbaya Supardan 2<sup>a,b</sup>, Rozan Mohammad Yunus 3<sup>c</sup>, and Suraya Ahmad Kamil 4<sup>a,b\*</sup>

<sup>a</sup>Faculty of Applied Sciences, Universiti Teknologi MARA, 40450 Shah Alam, Selangor, Malaysia

<sup>b</sup>NANO-SciTech Lab (NST), Centre for Functional Materials and Nanotechnology (CFMN), Institute of Science (IOS), Universiti Teknologi MARA (UiTM), 40450 Shah Alam, Selangor, Malaysia

<sup>c</sup>Fuel Cell Institute, Universiti Kebangsaan Malaysia, 43600 Bangi, Selangor, Malaysia

\*Corresponding author. Tel.: +6019-4623195; fax: +603-55434562; e-mail: suraya\_ak@uitm.edu.my

Received 14 February 2023, Revised 17 May 2023, Accepted 25 May 2023

### ABSTRACT

SiO<sub>2</sub> and TiO<sub>2</sub> are often used in optical film due to their chemical stability and they have been proven as a favourable host for rare earth ions. Nanofiber has been widely studied because it possesses a high surface area per unit mass as well as low-cost production. In this study, sol-gel and electrospinning methods were used to synthesize and fabricate Er<sup>3+</sup>-doped SiO<sub>2</sub>-TiO<sub>2</sub> nanofiber with different ratios of SiO<sub>2</sub>/TiO<sub>2</sub>, respectively. The morphological, structural, and optical properties of the nanofiber were studied. The FESEM result shows that the produced fibers have diameters between 67 to 538 nm. The FTIR spectra imply that the main structure of the nanofiber remains unchanged despite the increasing of TiO<sub>2</sub> content in the host matrix. The obtained XRD results indicate that all samples correspond to the amorphous phase. Besides, the optical transparency of all the fabricated samples demonstrated a high transmittance (88% to 93%) which was ideal for photonic applications. The PL spectra showed strong green emission peaks associated to <sup>2</sup>H<sub>11/2</sub> → <sup>4</sup>I<sub>15/2</sub> of Er<sup>3+</sup> transitions under an excitation wavelength of 350 nm.

**Keywords:** SiO<sub>2</sub>-TiO<sub>2</sub>, Nanofiber, Photoluminescence, Optical materials, Rare-earth

### 1. INTRODUCTION

SiO<sub>2</sub> and TiO<sub>2</sub> are materials that are often used in optical film in the visible-near infrared wavelength range because of their chemical stability [1]. Both silicon dioxide and titanium dioxide are identified as low- and high-index materials, respectively. Due to the huge difference in refractive index between the two compounds, SiO<sub>2</sub>-TiO<sub>2</sub> composite materials are expected to have a wide range of refractive indices [2]. Furthermore, SiO<sub>2</sub>-TiO<sub>2</sub> thin film produced interesting characteristics such as high transparency, which make them ideal for potential optical applications [3]. Based on previous research, SiO<sub>2</sub>-TiO<sub>2</sub> mixed oxides have been preferred to be a host for rare earth ions [1, 4].

Rare earth ions act as active ions in solid-state luminescent materials. They are often used due to their unique spectral characteristics, which include absorbing and emitting in visible and infrared wavelengths [5, 6]. Rare earth-doped materials are of interest as they may provide unique and efficient luminescence characteristics as well as possible applications in optoelectronic technology [1, 6]. It is anticipated that the luminescence intensity of rare earth ions will increase greatly when they are incorporated into nanostructured materials [7]. Er<sup>3+</sup> ions have greater potential application in producing optical devices among rare earth ions [2]. Er<sup>3+</sup> exhibits photoluminescence at around 1.54 μm, which is among the common wavelengths

of the optical communication technology [3] that coincides with the low-loss window of silica-based optic fibers [1, 2, 8, 9]. Furthermore, Er<sup>3+</sup> is also of interest because of its intense luminescence within the visible light wavelength [10]. Several techniques, including rf-sputtering, chemical vapor deposition, ion exchange, sol-gel method, etc., can be used to dope Er<sup>3+</sup> into the host materials [1, 2, 5, 11].

Nanostructured materials (i.e., nanofibers, nanowires, nanoparticles, etc.) have been extensively studied by researchers due to their interesting optical properties. These nanostructured materials provide substantial advantages over the macroscale structures materials, which are lightweight, highly porous, and also have a high surface area to volume ratio, which may have a significant effect on their properties [5, 7, 12]. Nanofiber has been widely studied among these nanostructures because it is simple as well as its inexpensive fabrication [5]. Nanofibers can be produced by numerous techniques, including self-assembly, drawing, porous template, and electrospinning [7].

The electrospinning method has been used since the 1930s and is an efficient method to fabricate nanofibers [12, 13]. Electrospinning has been proven to be a simple, convenient, cost effective and versatile way [4, 14] to fabricate nanofibers with controllable sizes between tens of nanometers and micrometers [4, 7, 14]. The characteristics of the materials as well as the electrospinning parameters, such as the concentration and

viscosity of the solution, the applied voltage, the deposition distance and also humidity, determine the morphologies and properties of the nanofibers [7, 12, 13, 15]. Nanofibers with various morphologies, including ribbon, beaded, porous and core-shell fibers, can be produced by adjusting the parameters [4, 5, 7]. Recently, there has been growing interest in the fabrication of nanofiber by combining the sol-gel method and the electrospinning process [12]. SiO<sub>2</sub>-TiO<sub>2</sub> obtained using the sol-gel method have been widely studied because of their optical applications [3, 6, 16]. Numerous benefits such as homogeneity of the solution, low temperature processing, and controllable properties for instance, morphology of the nanofiber, can be produced from this combination [7].

In this study, Er<sup>3+</sup>-doped (x)SiO<sub>2</sub>-(100-x)TiO<sub>2</sub> with different amounts of x = 75, 85, 90, 95 and 100 mol% solutions were synthesized and fabricated using the sol-gel and electrospinning techniques, correspondingly. The morphological, structural, and optical properties of the nanofiber were studied and discussed.

## 2. METHODOLOGY

### 2.1. Synthesis of Er<sup>3+</sup>- Doped SiO<sub>2</sub>-TiO<sub>2</sub>

The TiO<sub>2</sub> sol (Solution A) was first synthesized by mixing titanium butoxide (Ti(OC<sub>4</sub>H<sub>9</sub>)<sub>4</sub>) with H<sub>2</sub>O. Then, hydrochloric acid (HCl) was added drop by drop into the solution and left to be stirred at 50°C with the stirring speed of 400 rpm for 24 hours. Next, SiO<sub>2</sub> sol (Solution B) was synthesized by mixing tetraethylorthosilicate (Si(OC<sub>2</sub>H<sub>5</sub>)<sub>4</sub>, TEOS) [98% Fluka], isopropanol (C<sub>3</sub>H<sub>8</sub>O) [99+% Aldrich], H<sub>2</sub>O and hydrochloric acid (HCl, 37% concentration) at 50°C for 2 hours with stirring speed of 400 rpm. Isopropanol and hydrochloric acid acted as solvents and catalysts, respectively. Certain amounts from each solution (Solution A and Solution B) were used to mix for different weight percent ratios of the sample. Next, erbium chloride, anhydrous (ErCl<sub>3</sub>, 99.9%), which acts as dopant, was first diluted with H<sub>2</sub>O, and then was added to the resultant solution (Solution A + Solution B). The amount of Er<sup>3+</sup> remained constant at 0.5 mol%. The ratio and doping percentages used for each sample are listed in Table 1.

**Table 1** Ratio and doping percentages used

Sample	Ratio and doping percentages used
Er <sup>3+</sup> -doped 100SiO <sub>2</sub>	100% SiO <sub>2</sub> - 0% TiO <sub>2</sub> (0.5 mol% Er <sup>3+</sup> )
Er <sup>3+</sup> -doped 95SiO <sub>2</sub> -5TiO <sub>2</sub>	95% SiO <sub>2</sub> - 5% TiO <sub>2</sub> (0.5 mol% Er <sup>3+</sup> )
Er <sup>3+</sup> -doped 90SiO <sub>2</sub> -10TiO <sub>2</sub>	90% SiO <sub>2</sub> - 10% TiO <sub>2</sub> (0.5 mol% Er <sup>3+</sup> )
Er <sup>3+</sup> -doped 85SiO <sub>2</sub> -15TiO <sub>2</sub>	85% SiO <sub>2</sub> - 15% TiO <sub>2</sub> (0.5 mol% Er <sup>3+</sup> )
Er <sup>3+</sup> -doped 75SiO <sub>2</sub> -25TiO <sub>2</sub>	75% SiO <sub>2</sub> - 25% TiO <sub>2</sub> (0.5 mol% Er <sup>3+</sup> )

The resultant mixture was stirred overnight at room temperature to obtain a transparent and homogenous solution. A spinnable solution for electrospinning was prepared by combining Er<sup>3+</sup>-doped (x)SiO<sub>2</sub>-(100-x)TiO<sub>2</sub> solution with polyvinyl alcohol (PVA). The incorporation of PVA into the mixture serves as a binder to enhance the solution's spinnability since it promotes the bonding of the particles in the solution. The mixture was then stirred for about 1 hour before the fabrication of the nanofiber.

### 2.2 Electrospinning of Nanofibers

The nanofibers were produced by using electrospinning technique. The syringe was first loaded with the spinnable solution. Then, a constant feeding rate of 0.5 ml/hour was set for the syringe pump. The fused silica and silicon wafer substrates were attached on the aluminium foil collector and 13 kV of voltage was applied. The tip of the needle was fixed at a distance of 10 cm from the collector. The fabricated time for each sample is around 1 hour. Afterwards, each sample was annealed at 950 °C for approximately 5 hours. In order to reach the corresponding thermal temperature of 950 °C, the temperature continued to rise at the rate of 5 °C/min from room temperature. The temperature was then maintained for one hour before constantly decreasing to room temperature at the rate of 10 °C/min. The temperature is set up to 950 °C to remove the hydroxide (OH) group in the nanofiber completely.

### 2.2 Samples Characterization

The morphology and element distribution of the fabricated samples were obtained by using Field Emission Scanning Electron Microscopy (FESEM) and Energy Dispersive Spectroscopy (EDS) (JOEL JSM-7600F), respectively. Image J software (Version 1.53k) was used to measure the diameters of the electrospun nanofiber. FTIR spectra in the range 4000-600 cm<sup>-1</sup> were recorded using a Thermo Nicolet-6700 FTIR spectrometer. The structural properties of the electrospun nanofiber were evaluated by XRD-diffraction (PANalytical X'pert PRO, DY-2536) with Cu-Kα radiation of a wavelength of 1.5406 Å. Scans were made from 5° to 90° (2θ) with 0.026° in step size. The optical transparency of the samples were recorded in the range of 200-2000 nm using a UV-VIS-NIR spectrometer (Varian Cary 5000, Palo Alto, CA, USA), at room temperature. Photoluminescence spectra were obtained at room temperature under 350 nm excitation wavelength by using FLS920 Edinburgh Instrument fluorescence spectrometer.

## 3. RESULTS AND DISCUSSION

The surface morphology of the electrospun Er<sup>3+</sup>-doped (x)SiO<sub>2</sub>-(100-x)TiO<sub>2</sub> fibers (x= 100, 95 and 75 mol%) at 20 kX and 5 kX magnification shown in Figure 1(a), (b) and (c). The prepared samples consisted of fibers with random fibers orientation and diameters between 67 nm and 538 nm. The FESEM images in Figure 1 showed that the diameter size of the nanofibers increases as the titania content increases.

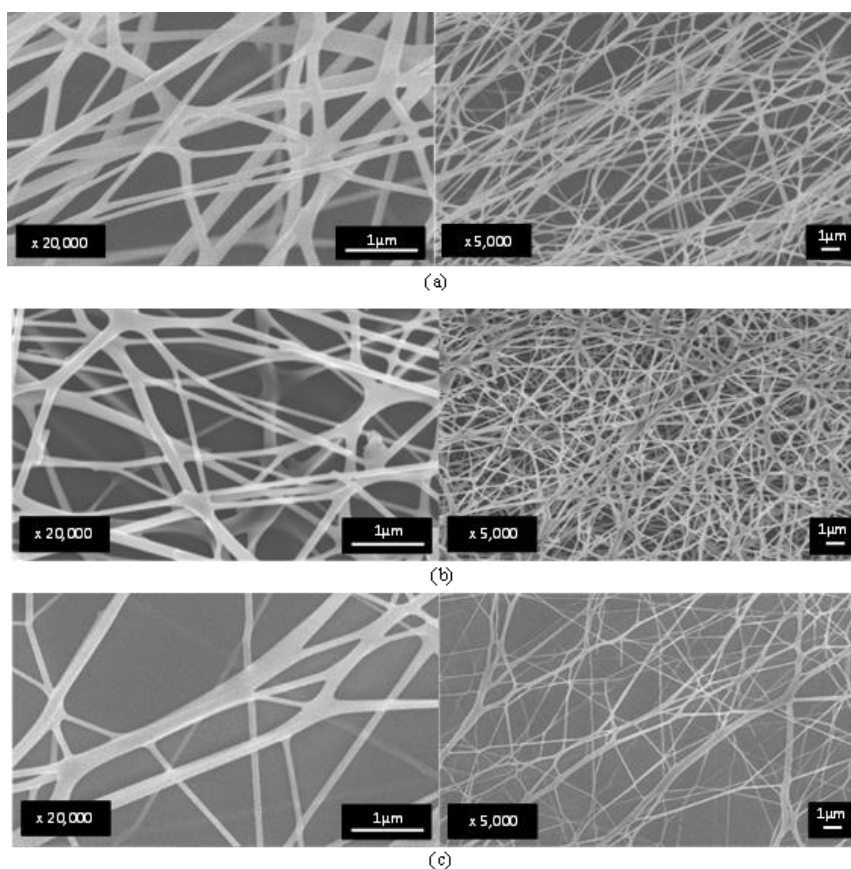


**Figure 1** The FESEM images of the fabricated nanofiber at the magnification of 20 kX and 5 kX for different ratio of TiO<sub>2</sub>; (a) 0 mol% TiO<sub>2</sub>; (b) 5 mol% TiO<sub>2</sub>; (c) 25 mol% TiO<sub>2</sub>

Table 2 presented the range of the nanofibers' diameter for Er<sup>3+</sup>-doped (x)SiO<sub>2</sub>-(100-x)TiO<sub>2</sub> (x= 100, 95 and 75 mol%) samples. The diameter can be seen increasing as the TiO<sub>2</sub> content increases. The increase in the nanofibers' diameter size may be caused by the increased viscosity of the spinnable solution that results from an increase in TiO<sub>2</sub> content. Previous study observed that introducing Ti- O<sub>2</sub> into SiO<sub>2</sub> solution caused the solution to become more viscous[17].

**Table 2** Nanofibers' diameter range of Er<sup>3+</sup>-doped SiO<sub>2</sub>-TiO<sub>2</sub> for different ratio.

Sample	Nanofibers' diameter range (nm)
Er <sup>3+</sup> -doped 100SiO <sub>2</sub>	67-440
Er <sup>3+</sup> -doped 95SiO <sub>2</sub> -5TiO <sub>2</sub>	75-467
Er <sup>3+</sup> -doped 75SiO <sub>2</sub> -25TiO <sub>2</sub>	80-538

In comparison to SiO<sup>4+</sup> (0.41 Å), TiO<sup>4+</sup> (0.61 Å) has a greater ionic radius [16, 18, 19]. As a result, the Ti-O bond's distance is greater (around 1.7-2.3 Å [20]) compared to Si-O bond at ~1.60 Å [18, 21]. A longer molecule is produced when there is a greater distance separating Ti particle.

These particles are prone to entangling, making it hard to move past one another. As a result, a larger inorganic network forms when the TiO<sub>2</sub> concentration is higher, making the nanofiber solution more viscous [17]. Changes in the fiber orientation and branching of the nanofiber might be generated by the multijet formed by the solution droplet or the unstable jet trajectory which was caused by the instability in electric field intensity towards the substrates [5, 13]. In addition, the surface morphology of the fibrous nanofiber remained smooth after been calcined at high temperature [5, 14].

The energy dispersed spectrum (EDS) mapping across the scanned area presented the ion distribution of Si, Ti, O and Er is shown in Figure 2 and the ions appears to be homogenously distributed within the host matrix [5]. Table 3 shows the elemental composition of Er<sup>3+</sup>-doped 90SiO<sub>2</sub>-10TiO<sub>2</sub>. The Si atomic percentage may not totally be contributed by Si ions. Part of it was probably contributed by the substrate on which the fiber is deposited.

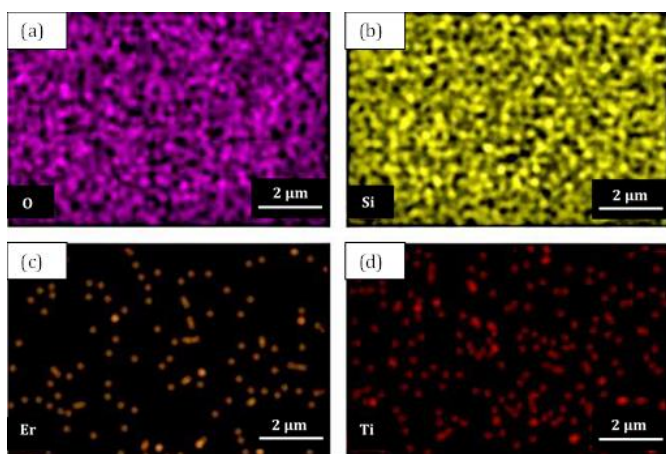


**Figure 2** EDS mapping of respective ions of (a) O; (b) Si; (c) Er; and (d) Ti in Er<sup>3+</sup>-doped 90SiO<sub>2</sub>-10TiO<sub>2</sub>

**Table 3** Elemental composition of Er<sup>3+</sup>-doped 90SiO<sub>2</sub>-10TiO<sub>2</sub>

Element	Weight %
O K	56.62
Si K	46.32
Ti K	1.45
Er L	0.22

Figure 3 shows the FTIR absorption spectra of Er<sup>3+</sup>-doped SiO<sub>2</sub>-TiO<sub>2</sub> nanofibers in the range of 600-4000 cm<sup>-1</sup>. The bands around ~ 970, 780, 1130 cm<sup>-1</sup> depicted the characteristics of silica as well as the formation of SiO<sub>2</sub> network [22]. The bands approximately around 970 cm<sup>-1</sup> are caused by the Si-O bending mode of non-bridging oxygen. The bands located at ~780 cm<sup>-1</sup> and near 1130 cm<sup>-1</sup> are attributed to the Si-O vibration and Si-O-Si bond, respectively [4, 13, 22].

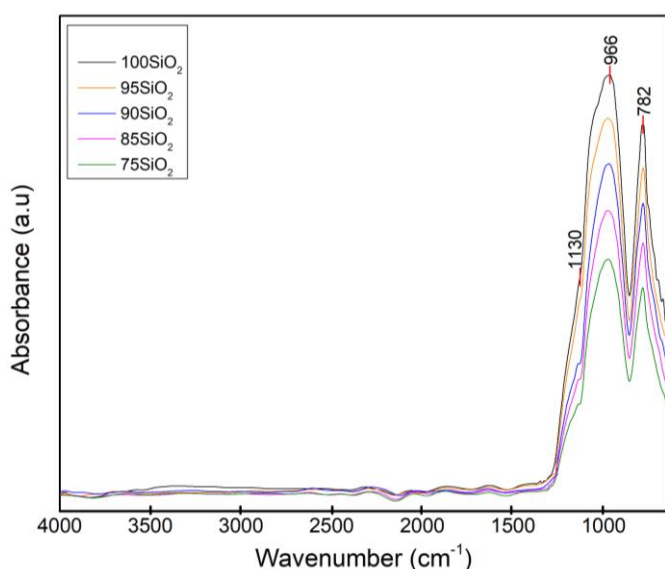


**Figure 3** FTIR spectra of Er<sup>3+</sup>-doped (x)SiO<sub>2</sub>-(100-x)TiO<sub>2</sub> fibers with different amount of x = 100, 95, 90, 85 and 75 mol%.

The FTIR spectra shows no peak around 3000-4000 cm<sup>-1</sup> indicates that OH group was fully removed after being annealed at 950°C [19, 22-24]. The presence of OH group might enhance the phonon energy level that increase the non-radiative de-excitation of Er<sup>3+</sup> that will significantly reduce the Er<sup>3+</sup> luminescence [25]. The FTIR spectra shown in Figure 3 revealed no peaks of Ti network as the peaks for all the sample were similar, including the sample with 0 mol% of TiO<sub>2</sub> content. This suggests that the main structure of the nanofiber has not changed although the content of TiO<sub>2</sub> in the host matrix increased. However, the intensity of the peak shown in the FTIR spectra decreased as the content of the SiO<sub>2</sub> decreased.

The XRD patterns of Er<sup>3+</sup>-doped SiO<sub>2</sub>-TiO<sub>2</sub> nanofiber with various SiO<sub>2</sub>/TiO<sub>2</sub> ratios are shown in Figure 4. A broad peak around 2θ=22° corresponds to the amorphous phase in the nanofiber [6, 12]. Zhao, J. et al. reported that when TiO<sub>2</sub>/SiO<sub>2</sub> ratio is less than 2, the samples showed typical amorphous glass pattern since no diffraction peak detected. Apart from that, there is also no additional phase or characteristics peak related to Er<sup>3+</sup> compound was found, which suggests that Er<sup>3+</sup> has been effectively integrated into SiO<sub>2</sub>-TiO<sub>2</sub> nanofiber [1, 26].

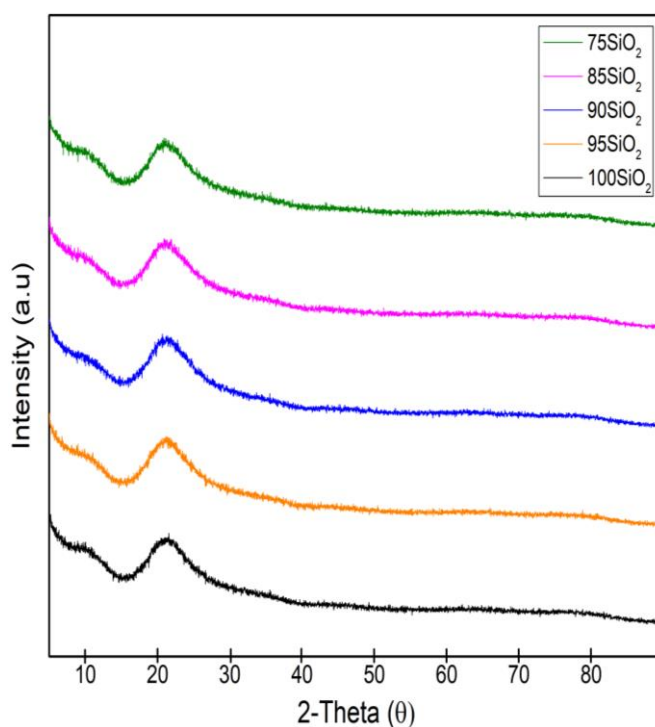


**Figure 4** XRD patterns of Er<sup>3+</sup>-doped (x)SiO<sub>2</sub>-(100-x)TiO<sub>2</sub> nanofibers with different ratio of TiO<sub>2</sub>: (a) 0 mol%; (b) 5 mol%; (c) 10 mol%; (d) 15 mol% and (e) 25 mol% of TiO<sub>2</sub>.

The optical transparency of the sample in Figure 5 showed that the transmission spectra of all the fabricated samples had high transmission spectra in UV-VIS-NIR wavelength range and exhibited similar spectral patterns. A range of about 88% to 93% transmittance demonstrates that all the samples possessed high optical transparency which makes them ideal for photonic applications [5, 25].

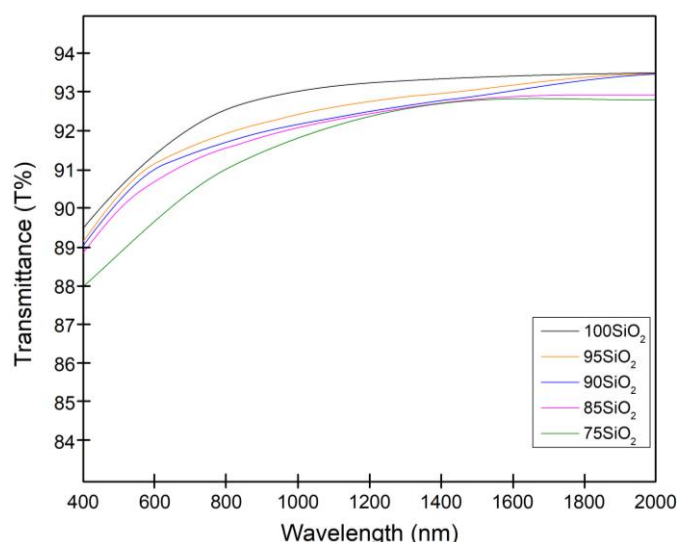


**Figure 5** Transmittance of Er<sup>3+</sup>-doped SiO<sub>2</sub>-TiO<sub>2</sub> nanofibers in the range of 400-2000 nm

Figure 6 shows the PL spectral emission of the samples under 350 nm excitation wavelength. The PL spectra showed peaks around 453 nm, ~509 nm, ~521 nm, and ~570 nm associated with Er<sup>3+</sup> ions. The PL intensity exhibit a blue emission band of  $^4F_{5/2} \rightarrow ^4I_{15/2}$  at 453 nm. The intense green emission peak observed at 509 nm and 521 nm ascribed to the  $^2H_{11/2} \rightarrow ^4I_{15/2}$  Er<sup>3+</sup> transition while a weak broad peak around ~570 nm is attributed to the  $^4S_{3/2} \rightarrow ^4I_{15/2}$  transition of Er<sup>3+</sup> ions [25, 27, 28]. The emission at 453 nm and the weak broad peak around 570 nm are most likely due to the surface defect produced by the host-related defect levels. The host band gap developed a defect level as a result of the Er<sup>3+</sup> ions dopants. Defects or vacancies will increase when the host ions are replaced with rare earth ions. Therefore, it will enhance the energy transfer from the band edge to the defect level for the visible emission [28-30]. In contrast, at greater SiO<sub>2</sub> concentrations, the Er<sup>3+</sup> ions are located at defects, vacancies or on the surface whereas the samples with higher content of TiO<sub>2</sub> exhibit stronger emissions [31]. This occurrence is most likely caused by the presence of TiO<sub>2</sub> which serves as network modifier [18, 32, 33] to increase the number of non-bridging oxygen (NBO) bonds available to be bonded with RE ions.

#### 4. CONCLUSIONS

The morphological, structural, and optical characterization of Er<sup>3+</sup>-doped SiO<sub>2</sub>-TiO<sub>2</sub> nanofibers are reported in this paper. This work has shown that the nanofibers' diameter increases as the TiO<sub>2</sub> concentration increases. This might be due to the solution's high viscosity when a greater amount of TiO<sub>2</sub> was introduced into the spinnable solution. The FTIR spectra show similar trends for all samples. The obtained XRD results show that all the samples were in an amorphous phase. The optical transparency of all the fabricated samples showed high transmittance (88% to 93%), which were ideal for photonic applications. The PL intensity exhibits a blue emission band of  $^4F_{5/2} \rightarrow ^4I_{15/2}$  at 453 nm and a weak broad peak in the green region around ~570 nm, associated with the surface defects caused by Er<sup>3+</sup> ions. The intense green emission is observed at 509 nm

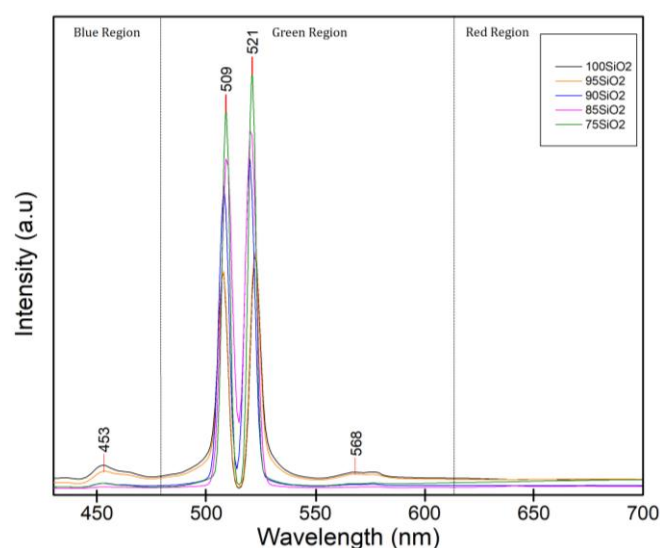


**Figure 6** PL of the Er<sup>3+</sup>-doped SiO<sub>2</sub>-TiO<sub>2</sub> under 350 nm excitation.

and 521 nm, ascribed to the  $^2H_{11/2} \rightarrow ^4I_{15/2}$  transition of Er<sup>3+</sup> ions.

#### ACKNOWLEDGMENTS

The project was financially supported by the Ministry of Education of Malaysia and Research Management Centre (RMC), Universiti Teknologi MARA through the Fundamental Research Grant Scheme (FRGS, Sponsorship File No. FRGS/1/2019/STG02/UITM/02/11; 600-IRMI/FRGS 5/3 (431/2019)).

#### REFERENCES

- [1] J. Zhao, et al., "Visible erbium luminescence in Er<sup>3+</sup>-doped SiO<sub>2</sub>-TiO<sub>2</sub> films prepared by sol-gel method," *Journal of Optoelectronics and Advanced Materials*, 2011.
- [2] J.S. Jeng, L.L. Yang, J.S. Chen, "Light emission and atomic coordination structure of sol-gel derived erbium-doped SiO<sub>2</sub>-TiO<sub>2</sub> thin films," *Thin Solid Films*, 2017, vol. 640, pp. 20-26.
- [3] Q. Fang, et al., "FTIR and XPS investigation of Er-doped SiO<sub>2</sub>-TiO<sub>2</sub> films," *Materials Science and Engineering: B*, 2003, vol. 105, no. 1-3, pp. 209-213.
- [4] J. Li, et al., "Excellent Flexibility of High-Temperature-Treated SiO<sub>2</sub>-TiO<sub>2</sub> Hybrid fibres and their enhanced luminescence with Eu<sup>3+</sup> doping," *Ceramics International*, 2017, vol. 43, no. 15, pp. 12710-12717.
- [5] M.K. Abd-Rahman, N.I. Razaki, "Effect of Nanofiber/Thin-Film Multilayers on the Optical Properties of Thulium-Doped Silica-Alumina," *Journal of Luminescence*, 2018, vol. 196, pp. 442-448.
- [6] J.G. Zhao, et al., "Structure and photoluminescence properties of Er<sup>3+</sup>-doped TiO<sub>2</sub>-SiO<sub>2</sub> powders

- prepared by sol–gel method,” *Chinese Physics B*, 2011, vol. 20, no. 8.
- [7] N.I. Razaki, M.K. Abd-Rahman, “Preparation and Characterization of Thulium Doped Silica-Alumina Nanofibers for Photonics Application,” 2017.
- [8] N.I. Razaki, S.A. Kamil, M.K. Abd-Rahman, “Optical and Morphological Properties of SiO<sub>2</sub>-PVA and Er<sup>3+</sup>doped SiO<sub>2</sub>-PVA Thin Film and Nanofibers,” *International Journal of Nanoelectronics and Materials*, 2020.
- [9] L. Predoana, et al., “Nanostructured Er<sup>3+</sup>doped SiO<sub>2</sub>-TiO<sub>2</sub> and SiO<sub>2</sub>-TiO<sub>2</sub>-Al<sub>2</sub>O<sub>3</sub> sol–gel thin films for integrated optics,” *Optical Materials*, 2015, vol. 46, pp. 481-490.
- [10] L.M. Lozano-Sánchez, et al., “Visible and near-infrared light-driven photocatalytic activity of erbium-doped CaTiO<sub>3</sub> system,” *Journal of Molecular Catalysis A: Chemical*, 2015, vol. 410, pp. 19-25.
- [11] P. Karasinski, et al., “Two-Component Waveguide SiO<sub>2</sub>-TiO<sub>2</sub> Films Fabricated by Sol–Gel Technology for Optoelectronic Applications,” 2014.
- [12] S.W. Lee, et al., “Preparation of SiO<sub>2</sub>/TiO<sub>2</sub> composite fibers by sol–gel reaction and electrospinning,” *Materials Letters*, 2007, vol. 61, no. 3, pp. 889-893.
- [13] B. Ding, et al., “Morphology and Crystalline Phase Study of Electrospun TiO<sub>2</sub>-SiO<sub>2</sub> Nanofibres,” 2003.
- [14] L. Cui, et al., “Electrospinning Synthesis of SiO<sub>2</sub>-TiO<sub>2</sub> Hybrid Nanofibers with Large Surface Area and Excellent Photocatalytic Activity,” *Applied Surface Science*, 2019, vol. 488, pp. 284-292.
- [15] M.K. Abd-Rahman, et al., “Optical Characteristics of Erbium-Doped SiO<sub>2</sub>/PVA Electrospun Nanofibers,” *Advanced Materials Research*, 2015, vol. 1108, pp. 59-66.
- [16] I. Zaręba-Grodź, et al., “Europium-doped silica-titania thin films obtained by the sol–gel method,” *Optical Materials*, 2007, vol. 29, no. 8, pp. 1103-1106.
- [17] F. Huang, et al., “Electrospinning Amorphous SiO<sub>2</sub>-TiO<sub>2</sub> and TiO<sub>2</sub> Nanofibers Using Sol-Gel Chemistry and its Thermal Conversion Into Anatase and Rutile,” *Ceramics International*, 2018, vol. 44, no. 5, pp. 4577-4585.
- [18] Z. Pang, et al., “The effect of TiO<sub>2</sub> on the thermal stability and structure of high acidity slag for mineral wool production,” *Journal of Non-Crystalline Solids*, 2021, vol. 571.
- [19] C.F. Song, et al., “Structure and photoluminescence properties of sol–gel TiO<sub>2</sub>-SiO<sub>2</sub> films,” *Thin Solid Films*, 2002.
- [20] Y. Peng, et al., “Pivotal role of Ti-O bond lengths on crystalline structure transition of sodium titanates during electrochemical deoxidation in CaCl<sub>2</sub>NaCl melt,” *Journal of Alloys and Compounds*, 2018, vol. 738, pp. 345-353.
- [21] H.R. Philipp, “Optical properties of non-crystalline Si, SiO, SiO<sub>x</sub> and SiO<sub>2</sub>,” 1971.
- [22] R.R. Gonçalves, et al., “Active Planar Waveguides Based on Sol–Gel Er<sup>3+</sup>Doped SiO<sub>2</sub>-ZrO<sub>2</sub> for Photonic Applications: Morphological, Structural and Optical Properties,” *Journal of Non-Crystalline Solids*, 2008, vol. 354, no. 42-44, pp. 4846-4851.
- [23] W.Y. Wang, H.Y. Lee, C.L. Chung, “Preparation of Si-Ti Based Nanofibers and Thin Film by Single-Needle Electrospinning,” 2019.
- [24] S.I. Seok, et al., “Optical Properties of Er-Doped Al<sub>2</sub>O<sub>3</sub>-SiO<sub>2</sub> Films Prepared by a Modified Sol-Gel Process,” *Journal of the American Ceramic Society*, 2005, vol. 88, no. 9, pp. 2380-2384.
- [25] S.A. Kamil, et al., “Optical and Structural Properties of Er<sup>3+</sup>doped SiO<sub>2</sub>-ZrO<sub>2</sub> Glass-Ceramic Thin Film,” *Journal of Physics: Conference Series*, 2019.
- [26] J.S. Jeng, L.L. Yang, J.S. Chen, “Light Emission and Atomic Coordination Structure of Sol-Gel Derived Erbium-doped SiO<sub>2</sub>-TiO<sub>2</sub> Thin Films,” *Thin Solid Films*, 2017, vol. 640, pp. 20-26.
- [27] P. Singh, et al., “Photoluminescence Property of Erbium-Doped Yttrium Oxide: Doping Concentration and Its Effect,” *Integrated Ferroelectrics*, 2022, vol. 230, no. 1, pp. 100-107.
- [28] B. Chang-Hyuck, L. Ki-Soo, “Enhanced Blue Emission in Er<sup>3+</sup>/Yb<sup>3+</sup> Doped Glass-ceramics Containing Ag Nanoparticles and ZnO Nanocrystals,” *Current Optics and Photonics*, 2019.
- [29] X.-H. Zhang, et al., “A simple route to fabricate high sensibility gas sensors based on erbium doped ZnO nanocrystals,” *Colloids and Surfaces A: Physicochemical and Engineering Aspects*, 2011, vol. 384, no. 1-3, pp. 580-584.
- [30] C.-H. Wen, et al., “Red, green and blue photoluminescence of erbium doped potassium tantalate niobate polycrystalline,” *Journal of Alloys and Compounds*, 2008, vol. 459, no. 1-2, pp. 107-112.
- [31] J.M.M. Buarque, et al., “SiO<sub>2</sub>-TiO<sub>2</sub> Doped with Er<sup>3+</sup>/Yb<sup>3+</sup>/Eu<sup>3+</sup> Photoluminescent Material: A Spectroscopy and Structural Study About Potential Application for Improvement of the Efficiency on Solar Cells,” *Materials Research Bulletin*, 2018, vol. 107, pp. 295-307.
- [32] J. Park, A. Ozturk, “Effect of TiO<sub>2</sub> addition on the crystallization and tribological properties of MgO-CaO-SiO<sub>2</sub>-P<sub>2</sub>O<sub>5</sub>-F glasses,” *Thermochimica Acta*, 2008, vol. 470, no. 1-2, pp. 60-66.
- [33] M.V.S. Alencar, et al., “Structure, Glass Stability and Crystallization Activation Energy of SrO-CaO-B<sub>2</sub>O<sub>3</sub>-SiO<sub>2</sub> glasses doped with TiO<sub>2</sub>,” *Journal of Non-Crystalline Solids*, 2021, vol. 554.